Journal of Marine Systems 234 (2022) 103775

Contents lists available at ScienceDirect

Journal of Marine Systems

journal homepage: www.elsevier.com/locate/jmarsys

Decadal trends in Ocean Acidification from the Ocean Weather Station M in the Norwegian Sea

Ingunn Skjelvan [a,*], Siv K. Lauvset [a], Truls Johannessen [b], Kjell Gundersen [c], Øystein Skagseth [c]

[a] NORCE Norwegian Research Centre, Bjerknes Center for Climate Research, Jahnebakken 5, NO-5007 Bergen, Norway
[b] Geophysical Institute, University of Bergen, Allegaten 70, NO-5007 Bergen, Norway
[c] Institute of Marine Research, PO Box 1870 Nordnes, NO-5817 Bergen, Norway

ARTICLE INFO

Keywords:
Time series
Carbon
Ocean acidification
Trends
Nordic seas
Norwegian Sea
In situ observations
66°N 2°E

ABSTRACT

The Ocean Weather Station M (OWSM) is situated at a fixed position in the Norwegian Sea, one of the major basins of the Nordic Seas, which represents an important area for uptake of atmospheric CO_2 as well as deep water formation. At OWSM, the inorganic carbon cycle has been regularly monitored since 2001, and significant interannual changes of the carbonate system have been determined. Data collected at this site since the 1990s have been included, and over the 28 last years the surface fugacity of CO_2 (fCO_2) has increased by 2.92 ± 0.37 μatm yr^{-1}, while surface pH and aragonite saturation (Ω_{Ar}) have decreased by −0.0033 ± 0.0005 yr^{-1} and −0.018 ± 0.003 yr^{-1}, respectively. This corresponds to a surface pH change of −0.092 over 28 years, which is comparable to the global mean pH decrease of −0.1 since the onset of the industrial revolution. Our estimates suggest that 80% of the surface pH trend at OWSM is driven by uptake of CO_2 from the atmosphere. In the deepest layer, Ω_{Ar} has decreased significantly (−0.006 ± 0.001 yr^{-1}) over the last 28 years, now occasionally reaching undersaturated values ($\Omega_{Ar} < 1$). As a rough estimate, the saturation horizon has shoaled by 7 m yr^{-1} between 1994 and 2021. The increase in surface fCO_2 is confirmed by semi-continuous measurements of CO_2 from the site (2.69 ± 0.14 μatm yr^{-1}), and thus, the area has become less of a net sink for atmospheric CO_2, taking into consideration an atmospheric CO_2 increase at OWSM of 2.27 ± 0.08 μatm yr^{-1}.

1. Introduction

Friedlingstein et al. (2020) report that during the last decade a significant amount of carbon has been released into the atmosphere from fossil fuel combustion (9.4 ± 0.5 Pg C yr^{-1}) and due to land use change (1.6 ± 0.7 Pg C yr^{-1}). Of this anthropogenic carbon, about a quarter has been absorbed by the ocean annually (2.5 ± 0.6 Pg C yr^{-1}). This is a matter for concern since, over long term, absorbed CO_2 is perturbing the natural marine inorganic carbon cycle, where loss of carbonate (CO_3^{2-}) is increasing H^+ ion concentrations and reducing the pH of the ocean:

$$CO_2(aq) + H_2O \rightarrow H^+ + HCO_3^- \quad (1)$$

$$H^+ + CO_3^{2-} \rightarrow HCO_3^- \quad (2)$$

Further, a consumption of CO_3^{2-} lowers the ratio between dissolved carbonate ion and the saturation concentration of carbonate ion in seawater, which is defined as the saturation state of calcium carbonate (Ω). Of the two forms of calcium carbonate minerals apparent in seawater (calcite and aragonite), we focus on aragonite, which is the most soluble form. The combined effect of reduction in pH and Ω is commonly referred to as ocean acidification, OA (e.g., Gattuso and Hansson, 2012). In waters with $\Omega < 1$, the seawater is undersaturated with respect to calcium carbonate, and thus, the health of calcifying organisms is at potential risk (Kleypas et al., 2006; Doney et al., 2009).

Over the last century, the global pH has decreased by 0.1, which reflects an increase in the hydrogen ion concentration, $[H^+]$ of nearly 30% (Gattuso and Lavigne, 2009). The Arctic is assumed to experience the largest pH changes in this century (Steinacher et al., 2009; Chierici and Fransson, 2009). This is connected to the combined effect of temperature and salinity: cold water can hold more CO_2 than warm water and fresher water has a weaker buffer capacity compared to more saline water. Thus, the concentration of carbonate ion is low in Arctic waters, and regions in the Arctic Ocean are undersaturated with respect to aragonite during summer season (Azetsu-Scott et al., 2010; Chierici and Fransson, 2009). The seasonal variability of the marine carbon cycle often exceeds changes caused by anthropogenic input. Therefore, time

* Corresponding author.
E-mail address: insk@norceresearch.no (I. Skjelvan).

https://doi.org/10.1016/j.jmarsys.2022.103775
Received 15 November 2021; Received in revised form 9 June 2022; Accepted 10 June 2022
Available online 16 June 2022

series are of particular importance when small anthropogenic signals are to be detected, as shown by e.g., Bates et al. (2014). They compared seven Atlantic and Pacific Ocean time series, spanning 15–30 years, with negative pH trends varying from −0.0013 yr^{-1} off New Zeeland (Currie et al., 2011) to −0.0026 yr^{-1} in the Irminger Sea (Ólafsson et al., 2009; Olafsson et al., 2010).

This paper focus on time series data from the fixed Ocean Weather Station M (OWSM) in the Norwegian Sea of the Nordic Seas (Fig. 1). OWSM is one of very few stations at high latitudes where inorganic carbon has been monitored over several decades. The Nordic Seas comprises a surface mixture of relatively warm and saline northwards flowing Atlantic Waters and cold and fresh southwards flowing Polar Water with origin in the Arctic (Hansen and Østerhus, 2000), and is one of few places where deep and intermediate water are formed and fed into the North Atlantic. In addition to heat, carbon is also transported into the Nordic Seas and the area represents the northern limb of the conveyor belt. Thus, OWSM is located in a key area to observe changes related to climate change.

Many trend studies of carbon evaluate the surface water only (e.g., Bates et al., 2014; Hartman et al., 2015). In the Nordic Seas, the water exchange between surface and deep waters is reflected in the chemical characteristics of the water at different depth layers, and thus, timeseries which include intermediate and deep-water data in addition to surface data are of particular value as they contribute to highlight the changing carbonate cycle within the whole water column. Changes in pH and Ω_{Ar} are seen throughout the water column (Fransner et al., 2021), however, the reasons for the observed changes might vary between the water mases.

Here, we use decades of carbon data from OWSM to examine the changes in the Norwegian Sea inorganic carbon cycle, with focus on temporal pH changes. The aim of this study was to estimate the rate of pH change and to understand the driving forces behind the observed changes.

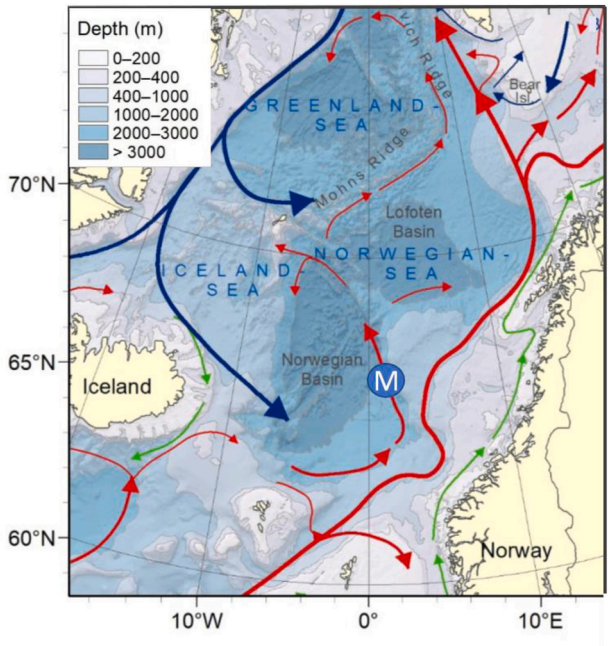

Fig. 1. The Nordic Seas in the northern North Atlantic with bathymetry, main currents (red = Atlantic water, blue = Arctic water, green = Coastal water), and position of OWSM. Modified from González-Pola et al., 2020. (For interpretation of the references to colour in this figure legend, the reader is referred to the web version of this article.)

2. Area

The Atlantic Water flows northwards via the Iceland Scotland ridge and into the Norwegian Sea (Fig. 1) primarily as a two branched current: the Norwegian Atlantic Current (NAC). The eastern branch follows the bathymetry of the Norwegian continental slope on its way northwards, while the western branch is characterized as an unstable frontal jet located above the 2000 m isobath (Orvik et al., 2001; Nilsen and Falck, 2006). The Atlantic Water is saline and carries large amounts of heat and carbon, which will be lost and removed, respectively, from the sea surface when the waters cools and overturns further north (Blindheim and Østerhus, 2005). OWSM is situated at 66°N 2°E at the western branch of the northwards flowing NAC where the bottom depth is 2100 m. The Norwegian Sea Arctic Intermediate Water, which is a mixture of upper Polar Deep Water, Iceland Sea Arctic Intermediate Water, and Greenland Sea Artic Intermediate Water (Jeansson et al., 2017), occupies the depth below the Atlantic Water. The area is highly dynamic, and the depth of the transition layer between Atlantic Water and Norwegian Sea Arctic Intermediate water can vary significantly (200–600 m) over short time (Mosby, 1962). However, in general, the Atlantic Water, with temperature > ~3 °C and salinities >35, occupies the upper 300–400 m at the OWSM site. The Norwegian Sea Deep Water is found at depths below 1000 m, and in between these water masses is the Norwegian Sea Arctic Intermediate Water. In general, the mixed layer depth (MLD) at OWSM varies between 20 m during summertime and 300 m during winter (Nilsen and Falck, 2006; Skjelvan et al., 2008).

3. Data

OWSM started in 1948 as the northernmost of 13 ocean weather stations in the North Atlantic. Weather ships, of which M/S Polarfront was the last, operated the station until 2009. From 2010 and onwards the station has been visited typically 5–6 times every year by research vessels from the fleet of the Norwegian Institute of Marine Research. From 1994 and onwards, the intermediate and deep water at the site have also been monitored by use of moored instruments, and between 2011 and 2021 a surface buoy (Polarbuoy) was deployed at the site. The various variables collected at the station are described below and in Table S1.

3.1. Discrete samples

Temperature and salinity have been measured over the full water depth at OWSM for >70 years (Østerhus and Gammelsrød, 1999; Nilsen and Falck, 2006), and presently, these variables are determined using a Sea-Bird Electronics (SBE) 911plus CTD calibrated towards bottle salinity samples. The salinity calibration samples are analysed on a Guildline Portasal Salinometer to an accuracy of ±0.003. Dissolved Inorganic Carbon (DIC) and Total Alkalinity (TA) have been monitored monthly between 2001 and 2009, and approximately every 2 months from 2010 onwards. The DIC and TA samples, which in general have been collected at 12 depth levels between surface and bottom, were conserved with saturated mercury chloride ($HgCl_2$) solution and analysed on shore following standard operational procedures (SOP, Dickson et al., 2007). DIC was determined by coulometric titration (SOP 2, Dickson et al., 2007; Johnson et al., 1993) thoroughly described in Skjelvan et al. (2008), while TA was measured using two versions of potentiometric open cell titration (SOP 3a, Dickson et al., 2007): one described in Haraldsson et al. (1997) for samples between 2001 and 2003 and another described in Mintrop et al. (2000) for samples from 2005 and onwards. Certified reference material (CRM) supplied by A. Dickson, Scripps Institution of Oceanography, USA, was regularly used to determine the accuracy of the measurements. For both DIC and TA the precision was determined to ±2.0 μmol kg^{-1}, based on duplicate samples. The discrete carbon data from OSWM are made available in GLODAPv2.2020 (Olsen et al., 2020). Comparison of deep-water TA

from OWSM over the last two decades indicated an offset of the 2001–2003 TA data, and, consequently, these early data have been corrected by +50 μmol kg^{-1}. The spread of the deep-water TA data was larger (2288–2316 μmol kg^{-1} at 2000) compared to other cruises in the Nordic Seas (Olsen, 2009). The measured TA data was compared with TA calculated from the TA-SSS (sea surface salinity) relationship of Nondal et al. (2009) where TA = 49.35* SSS + 582 (for salinity >34.5). The measured TA is equally distributed around the calculated TA (Fig. S1 in Supplementary material) with an average difference of −2.5 μmol kg^{-1} with a standard error of ±0.2 μmol kg^{-1}. Therefore, when TA data was lacking, TA was calculated from salinity.

From 1990, macronutrients from OWSM were measured weekly and from 2010 the frequency was reduced to 4–5 times per year. Dissolved inorganic nutrient concentrations were determined by standard colorimetric methods on an automated nutrient analyser (see Gundersen et al., 2021, for details). Briefly, nitrate and silicate are measured with a precision of <0.2% and has a calculated accuracy of ±1% at concentrations ranging from 0.5 to 20 μmol kg^{-1} (nitrate) and 0.7–20 μmol kg^{-1} (silicate). Since 2017, the range of concentrations was expanded to 0.5–50 μmol kg^{-1} for nitrate and 0.7–150 μmol kg^{-1} silicate. Phosphate is measured with a precision of <2% and an accuracy of ±2% at concentrations 0.05–3 μmol kg^{-1} (expanded to 0.05–5 μmol kg^{-1} in 2017).

Between 1981 and 2009, air samples were collected in glass flasks from M/S Polarfront at OWSM twice a week and analysed for CO_2 by NOAA/ESRL (Dlugokencky et al., 2021; Tans and Conway, 2005). The data between 2002 and 2009 are used here.

3.2. Semi-continuous samples

Semi-continuous measurements (once every 5 min or so) of sea surface fCO_2 at OWSM were performed onboard M/S Polarfront between 2005 and 2009 and from a surface buoy (Polarbuoy) between 2011 and 2021. At M/S Polarfront, the fCO_2 measurements were performed according to Pierrot et al. (2009), with shower head equilibration, non-dispersive infrared detection (LI-COR 6262), and frequent (every 3 h) use of three reference gases, and traceable to reference standards from National Oceanographic and Atmospheric Administration/Earth System Research Laboratory (NOAA/ESRL), of concentrations approximately 200, 350, and 420 ppm CO_2. Approximately once a day, the LI-COR was forced to adjust the zero and span using nitrogen with zero CO_2 and the reference gas with highest CO_2 concentration. Sea surface and equilibrator temperatures were continuously determined using Heart Scientific 1521 instruments with 5610 probes (precision ±0.01 °C), while the sea surface salinity was determined using a SBE 45 micro thermosalinograph (precision ±0.01 °C) calibrated towards weekly bottle salinity samples analysed at a Guildline Portasal Salinometer (model 8410A) to an accuracy of ±0.003 psu. The water intake for the system was at approximately 3 m depth. The accuracy of the fCO_2 data was ±2 μatm, and the data is available at https://www.socat.info/ (Bakker et al., 2016). Atmospheric measurements were performed using the same instrument at a frequency of once every 4 h and at an accuracy of ±1 μatm.

The Polarbuoy deployed at OWSM (2011−2021) was equipped with the Moored Autonomous pCO_2 ($MAPCO_2$) system. The system is thoroughly described in Sutton et al. (2014), and here only a brief description is included. Partially dried xCO_2 from approximately 0.5 m depth was measured using a bubble equilibrator (Friederich et al., 1995) and an infrared detector (LI-COR 820 CO_2 gas analyser), which was calibrated prior to every measurement using gas purged for CO_2 and a reference gas from NOAA/ERSL (order of 500 ppm CO_2). The $MAPCO_2$ system also included an air intake mounted approximately 1 m above sea surface, and measurements of sea surface and air pCO_2 were performed once every three hours. Sea surface temperature and salinity were determined using a SBE 37 MicroCAT, and these measurements were used to calculate the pCO_2 and fCO_2 according to Pierrot et al. (2009). The $MAPCO_2$ system delivers data with an accuracy in general better than ±5 μatm, and the data is available at https://www.socat.info/ (Bakker et al., 2016). The system performance has been compared with a General Oceanic pCO_2 system (Pierrot et al., 2009), similar to that used on M/S Polarfront, in the lab over 1.5 days with an average offset of 0.4 μatm and a standard error of 1.2 μatm.

3.3. Ancillary data

The discrete timeseries described above have been extended with three stations from 1994 (expocode 58AA19940826, station 7), 1998 (expocode 58JH19980801, station 485), and 2002 (expocode 216 N20020530, station 111) collected in the close vicinity of OWSM (65.6–66.4°N 1.7–2.3°E), where DIC and TA in addition to hydrography were collected and analysed using the same instruments as described above. These data are available from GLODAPv2.2020 (Olsen et al., 2020). Furthermore, atmospheric xCO_2 flask measurements from Mace Head, Ireland (Dlugokencky et al., 2021) were converted to $fCO2$ by using sea level pressure close to Mace Head downloaded from the NOAA ERDAP site (https://coastwatch.pfeg.noaa.gov/erddap/griddap/erdlasFnPres6.html) and sea surface temperature and salinity from OWSM.

4. Methods

pH at total scale, saturation state for the calcium carbonate mineral aragonite (Ω_{Ar}), and fCO_2 were calculated at in-situ temperature, salinity, and pressure using the carbon speciation software CO2SYS (van Heuven et al., 2011) with discrete DIC and TA data as input. In this calculation, the carbonate system constants from Lueker et al. (2000), the HSO_4^- constant from Dickson (1990), the total borate-salinity relationship of Uppström (1974), and the solubility product for calcite and aragonite, K_{sp}, from Mucci (1983) were used.

Interannual trends in temperature, salinity, DIC, TA, fCO_2, pH, and Ω_{Ar} have been determined by calculating annual averages of the measured discrete data over the depths 0–200 m, 200–500 m, 500–1000 m, and 1000–2100 m. These depth intervals are chosen based on a balance between vertical water mass extension and to ensure sufficient amount of data within each depth layer. The upper layer of 200 m is in general the depth which is influenced by seasonal variations. The trends were defined to be linear and significantly different from zero when the associated uncertainty was within the 95% confidence interval (based on *t*-test hypothesis). The standard error was calculated for each trend value. Trends in surface fCO_2 were also determined based on the semi-continuous surface data, where only months January to March were included to avoid influence of the biologically active seasons. These months were chosen because the winter mixed layer developed to its maximum values.

The drivers for the observed annual trend in pH were quantified by first assuming that the change in $[H^+]$ equals the sum of partial contributions from each of the drivers temperature (T), salinity (S), DIC, and TA:

$$\frac{d[H^+]}{dt} = \frac{\partial[H^+]}{\partial T}\frac{dT}{dt} + \frac{\partial[H^+]}{\partial S}\frac{dS}{dt} + \frac{\partial[H^+]}{\partial DIC}\frac{dDIC}{dt} + \frac{[H^+]}{\partial TA}\frac{dTA}{dt} \quad (3)$$

The partial derivatives of the above equation were determined by using the Matlab function derivnum as described in Orr et al. (2018). Their software package CO2SYS was modified from that of van Heuven et al. (2011). Further, the $[H^+]$ drivers were transformed into pH change by using the definition: $pH = -\log[H^+]$.

5. Results and discussion

5.1. Seasonality

The climatology of OWSM surface water (0–25 m) is shown in Fig. 2, where the monthly values are determined from averaging over the years 2001–2021. The surface water of OWSM is primarily affected by relatively warm and saline Atlantic Water, however, during late summer the

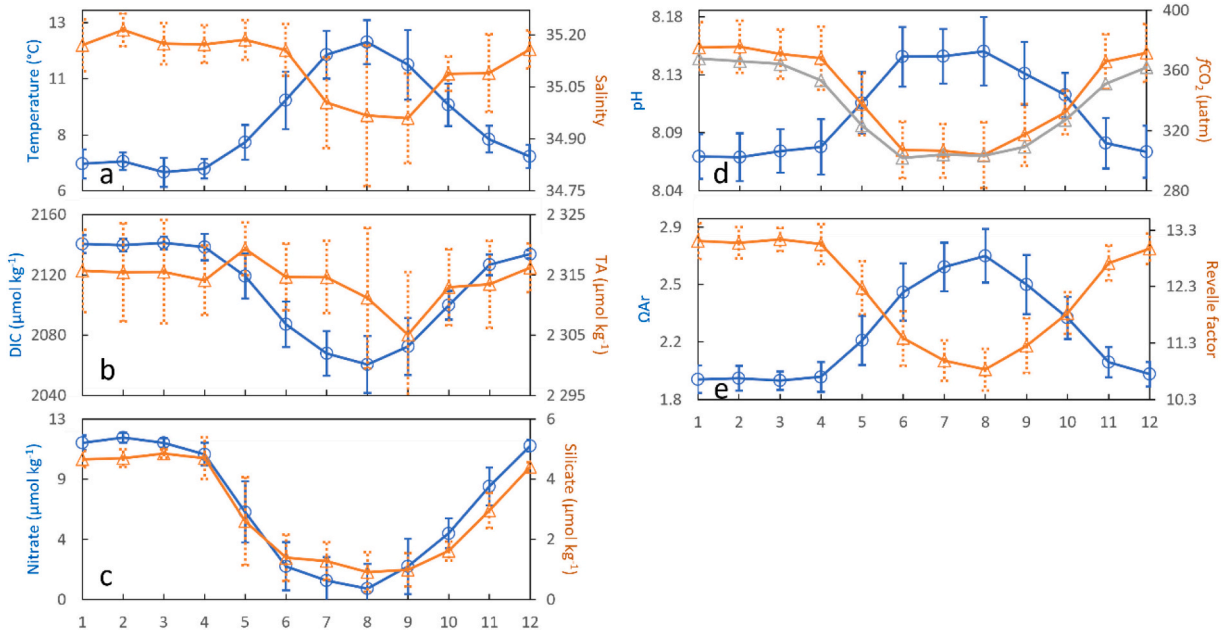

Fig. 2. Climatology of surface water (upper 25 m) of (a) temperature(°C) and salinity, (b) DIC (µmol kg^{-1}) and TA (µmol kg^{-1}), (c) nitrate (µmol kg^{-1}) and silicate (µmol kg^{-1}), (d) pH and fCO_2 (µatm), and (e) ΩAr and Revelle factor at OWSM calculated as monthly binned averages of the discrete timeseries (2001−2021). TA is calculated from salinity according to Nondal et al. (2009). The error bars represent one standard deviation. The grey triangles in panel (d) are monthly climatology of fCO_2 based on semi-continuous surface measurements performed onboard M/S Polarfront during 2006–2009.

salinity decreases due to intrusion of fresher water from the Norwegian Coastal Current (Fig. 2a). In April, surface DIC and nutrient concentrations decreased due to primary production and transfer of carbon into organic matter (Fig. 2b and c) leading to a decrease in fCO_2 (Fig. 2d). The timing and magnitude of the spring bloom is determined by several factors, where light is the most prominent factor, followed on a close second by thermal stratification of the water column. According to Dale et al. (1999), a pre-bloom accumulation of biomass starts in April in surface waters, while the main bloom event is beginning in May followed by a secondary short bloom in early fall. However, the latter is not visible in the climatology presented in Fig. 2. Nitrate and silicate concentrations appeared to be depleted equally but, although this was not examined further in this study, there is some skewness from a 1:1 M ratio between the two macronutrients. From the climatology (Fig. 2), there is no evidence of complete silicate or nitrate limitation in surface waters. However, observations show that, on occasion, nitrate concentration can reach zero at station OWSM. Findlay et al. (2008) and Moore et al. (2006) speculate that the lack of complete nutrient depletion in surface waters could be connected to iron limitation in this region.

The minimum levels of DIC and nutrients are reached in August. Further, the increasing pH during spring is a result of the combined effect of warmer water, which lowers the pH, and primary production, which increases pH. The latter effect dominates over the first during this time of year. Ω_{Ar} has a slightly slower response during the spring and increase, to some extent, with the increase in temperature. During fall, with cooling and deepening of the mixed layer, DIC and nutrients are remineralised from organic matter and are introduced into the surface layer, which, therefore, experiences increasing fCO_2. The winter mixed layer develops from further cooling and mixing and reaches its maximum depth usually in March. Typical winter values for surface water, the seasonal amplitudes, and the deep-water characteristics are presented in Table 1. The relatively low winter surface pH and Ω_{Ar} of 8.07 and 1.95, respectively, are comparable to the Icelandic timeseries (Ólafsson et al., 2009; Bates et al., 2014), which is dominated by cold Arctic Intermediate Water originating from mixing between Atlantic Water and low salinity Polar Water (Hansen and Østerhus, 2000). Thus, the lack of Polar Water at OWSM contribute to explaining the differences between seasonality at OWSM and at the Iceland and Irminger Sea time series.

Table 1
Water characteristics at OWSM based on data averaged over 2001–2021 (SD = standard deviation).

	Surface winter average ± 1 SD	Seasonal amplitude	Deep average ± 1 SD
Temperature (°C)	7.0 ± 0.6	5.2	−0.81 ± 0.03
Salinity	35.19 ± 0.06	0.23	34.913 ± 0.003
DIC (µmol kg^{-1})	2141 ± 5	81	2166 ± 3
TA (µmol kg^{-1})	2315 ± 9	8	2304 ± 7
fCO_2 (µatm)	373 ± 16	70	317 ± 12
pH	8.07 ± 0.02	0.08	8.03 ± 0.02
Ω_{Ar}	1.93 ± 0.07	0.76	1.00 ± 0.04
Revelle	13.1 ± 0.3	2.3	14.9 ± 0.3
NO_3 (µmol kg^{-1})	11.4 ± 0.4	10.6	14.7 ± 0.4
PO_4 (µmol kg^{-1})	0.77 ± 0.06	0.6	1.00 ± 0.05
Si (µmol kg^{-1})	4.7 ± 0.2	3.7	12.3 ± 0.5

Fig. 2d shows the seasonal fCO_2 amplitude of 65–73 µatm and confirms the expected similarity between calculated fCO_2 (from DIC and TA) and measured fCO_2. The Revelle factor (ocean buffer factor), which is defined as the fractional change in CO_2 relative to the fractional change in DIC, is high (13.1) in winter surface water at OWSM with a seasonal amplitude of approximately 2. This is characteristic for subpolar water and indicates that these waters have less capacity to absorb CO_2 from the atmosphere compared to waters further south.

The relatively large seasonal amplitudes observed at OWSM are comparable to those observed in the subpolar sites Irminger Sea and Iceland Sea located further west (Ólafsson et al., 2009; Bates et al., 2014) and at Porcupine Abyssal Plain (PAP) located further south in the Northeast Atlantic Ocean (Frigstad et al., 2015).

5.2. *Surface fCO_2 variability*

Fig. 3a shows time series of fCO_2 from semi-continuous

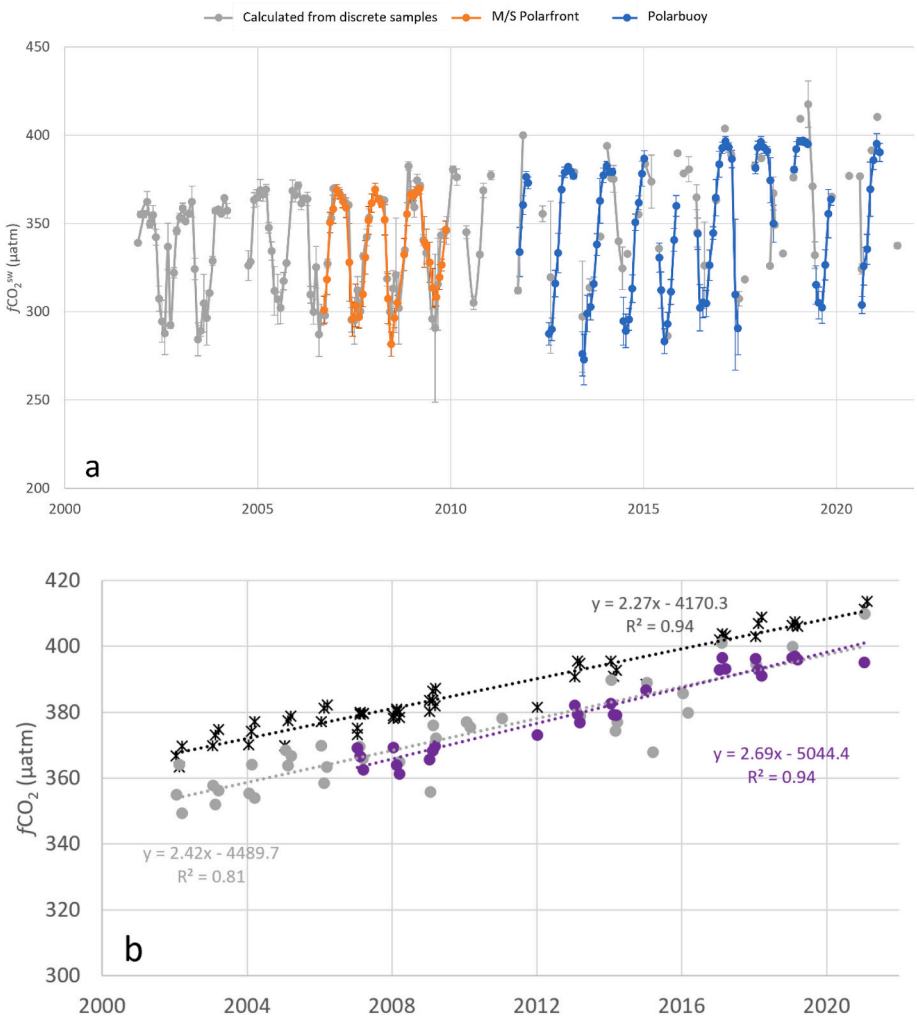

Fig. 3. a) Surface water variability of fCO_2^w over the years. Monthly averages from M/S Polarfront (red colour) and from the surface buoy (blue colour). Calculated fCO_2^w from discrete DIC and estimated TA (Nondal et al., 2009) from the upper 25 m (grey colour). Standard deviations of the monthly averages are shown. b) Monthly averages of January - March of atmospheric fCO_2 (fCO_2^a) from OWSM (black colour) and sea surface fCO_2 (grey and violet colour) as a function of years. The sea surface averages are based on continuous fCO_2 measurements onboard M/S Polarfront during 2007 - 2009 and continuous fCO_2^w measurements from the Polarbuoy between 2011 and 2021 (violet colour), and calculated fCO_2^w from the discrete DIC and estimated TA data over 0-200 m depth between 2001 and 2021 (grey colour). (For interpretation of the references to colour in this figure legend, the reader is referred to the web version of this article.)

measurements (M/S Polarfront and Polarbuoy) as well as fCO_2 calculated from discrete DIC and TA data from the upper 25 m. The seasonal variation is clearly seen with fCO_2 amplitudes varying from year to year and occasionally being larger (75–110 µatm) than the climatological fCO_2 amplitude of 70 µatm (Fig. 2d). Furthermore, the fCO_2 amplitudes seem to be increasing over the years and reached a maximum in the years 2013–2017. The limited amount of semi-continuous data makes it difficult to conclude regarding this matter, however, the temperature amplitude (Fig. S2) does not show such a pattern but rather fluctuates irregularly from year to year. Thus, the change in fCO_2 amplitudes could be connected to changes in the primary production and other non-thermal processes. According to multi-sensor satellite observations made available by Copernicus Marine Services (product identifier: OCEANCOLOUR_ATL_CHL_L3_REP_OBSERVATIONS_009_067; https://marine.copernicus.eu/access-data/ocean-monitoring-indicators/north-atlantic-ocean-chlorophyll-time-series-and-trend), the Chl-a concentration of the North Atlantic increased by $+0.17 \pm 0.013\%$ yr^{-1} over the years 1997–2019. It is reasonable to assume that this is also valid for the OWSM area, however, this needs to be confirmed by additional studies.

The seasonal oscillations are overlying a positive trend in surface water fCO_2 indicating an increasing content of CO_2 in the surface ocean, which is connected to the increasing atmospheric CO_2 concentrations. Fig. 3b shows monthly fCO_2 values from the winter season (January to March), and significant surface fCO_2 trends of $+2.69 \pm 0.14$ µatm yr^{-1} and $+ 2.42 \pm 0.20$ µatm yr^{-1}. These trends are determined from semi-continuous surface fCO_2 measurements during the years 2007–2021 and from fCO_2 calculated from discrete DIC and TA measurements in the upper 200 m during the years 2002–2021, respectively. The 200 m deep surface interval for the discrete samples was chosen because it is well within the winter mixed layer at the station. Moreover, Fig. 3b shows semi-continuous winter atmospheric fCO_2 (fCO_2^a) (January to March) data from OWSM determined from air flask samples from M/S Polarfront 2002–2009 (Dlugokencky et al., 2021), semi-continuous air samples from M/S Polarfront 2007–2009, and semi-continuous air samples from Polarbuoy between 2012 and 2021. The fCO_2^a winter trend of $+2.27 \pm 0.08$ µatm yr^{-1} is weaker than that of the semi-continuous fCO_2 data from the site ($+2.69 \pm 0.14$ µatm yr^{-1}), but within the uncertainty interval of the fCO_2 data calculated from discrete data ($+2.42 \pm 0.20$ µatm yr^{-1}). Thus, it is ambiguous if the site is a decreasing sink for atmospheric CO_2 or not. However, considering the uncertainty in calculating fCO_2 from DIC and TA, we have more confidence in comparing the directly measured fCO_2 in atmosphere and sea surface when it comes to determining the direction of ΔfCO_2. Thus, we conclude that the sea water fCO_2 at OWSM is increasing faster compared to that of the atmosphere and the area appears to be a decreasing sink for atmospheric CO_2. This conclusion is confirmed by replacing the atmospheric CO_2 data from OWSM with those from Mace Head, Ireland (Dlugokencky et al., 2021), of which the latter shows a winter trend in fCO_2 of $+2.12 \pm 0.07$ µatm yr^{-1} over the years 2002–2020, i.e., weaker than the trend in oceanic fCO_2 at the site.

The finding of OWSM being a decreasing sink for atmospheric CO_2 corresponds to results presented by e.g., Olsen et al. (2006), who explained the decreasing sink with an increasing amount of CO_2 in the surface water entering the Nordic Seas from the south due to a reduced

buffer capacity. This is in line with the decreasing buffer capacity calculated from OWSM timeseries data in the upper 200 m (not shown). Metzl et al. (2010) explained a strong positive trend in surface fCO_2 in the North Atlantic subpolar gyre with a) an increase in surface temperature over the period 1993–2003, and b) an increase in convection which increased the DIC/TA ratio during 2001–2008. Their increasing temperature observations were connected to changes in NAO (North Atlantic Oscillation) index from a positive to a negative phase.

b) Monthly averages of January–March of atmospheric fCO_2 (fCO_2^a) from OWSM (black colour) and sea surface fCO_2 (grey and violet colour) as a function of years. The sea surface averages are based on continuous fCO_2 measurements onboard M/S Polarfront during 2007–2009 and continuous fCO_2^w measurements from the Polarbuoy between 2011 and 2021 (violet colour), and calculated fCO_2^w from the discrete DIC and estimated TA data over 0–200 m depth between 2001 and 2021 (grey colour).

5.3. Water column variability and trends

Fig. 4 shows how a selection of variables is distributed and varies in the water column over two decades from 2001 to 2021. The seasonal signals in the uppermost 200 m seem to diminish during the last decade, however, this is an artefact due to lower sampling frequency between 2010 and 2021 than between 2001 and 2009. The winter mixed layer as shown in Skjelvan et al. (2008) varies between 250 and 350 m at the site, and no seasonal signals are seen below 200–300 m, which is similar to what was shown over a shorter period in Skjelvan et al. (2008). Fig. 4 shows that over the years, the intermediate and deep-water characteristics changes, with increasing DIC and fCO_2 and decreasing pH as the most prominent, but Ω_{Ar} is also decreasing over the years.

The interannual trends in four depth layers (0–200 m, 200–500 m, 500–1000 m, and 1000–2100 m) have been quantified and are presented in Fig. 5 and Table 2. DIC and fCO_2 are increasing significantly over the years (positive trend) in all depth layers, except for fCO_2 in the deepest layer. Furthermore, in all depth layers there are negative and significant trends in pH and Ω_{Ar}. The trends are strongest in the surface layer, where DIC, fCO_2, pH, and Ω_{Ar} change by $+1.48 \pm 0.22$ μmol kg^{-1} yr^{-1}, $+2.92 \pm 0.37$ μatm yr^{-1}, -0.0033 ± 0.0005 yr^{-1}, and -0.018 ± 0.003 yr^{-1}, respectively. The surface fCO_2 trend is within the uncertainty interval of the trend calculated from the semi-continuous winter surface

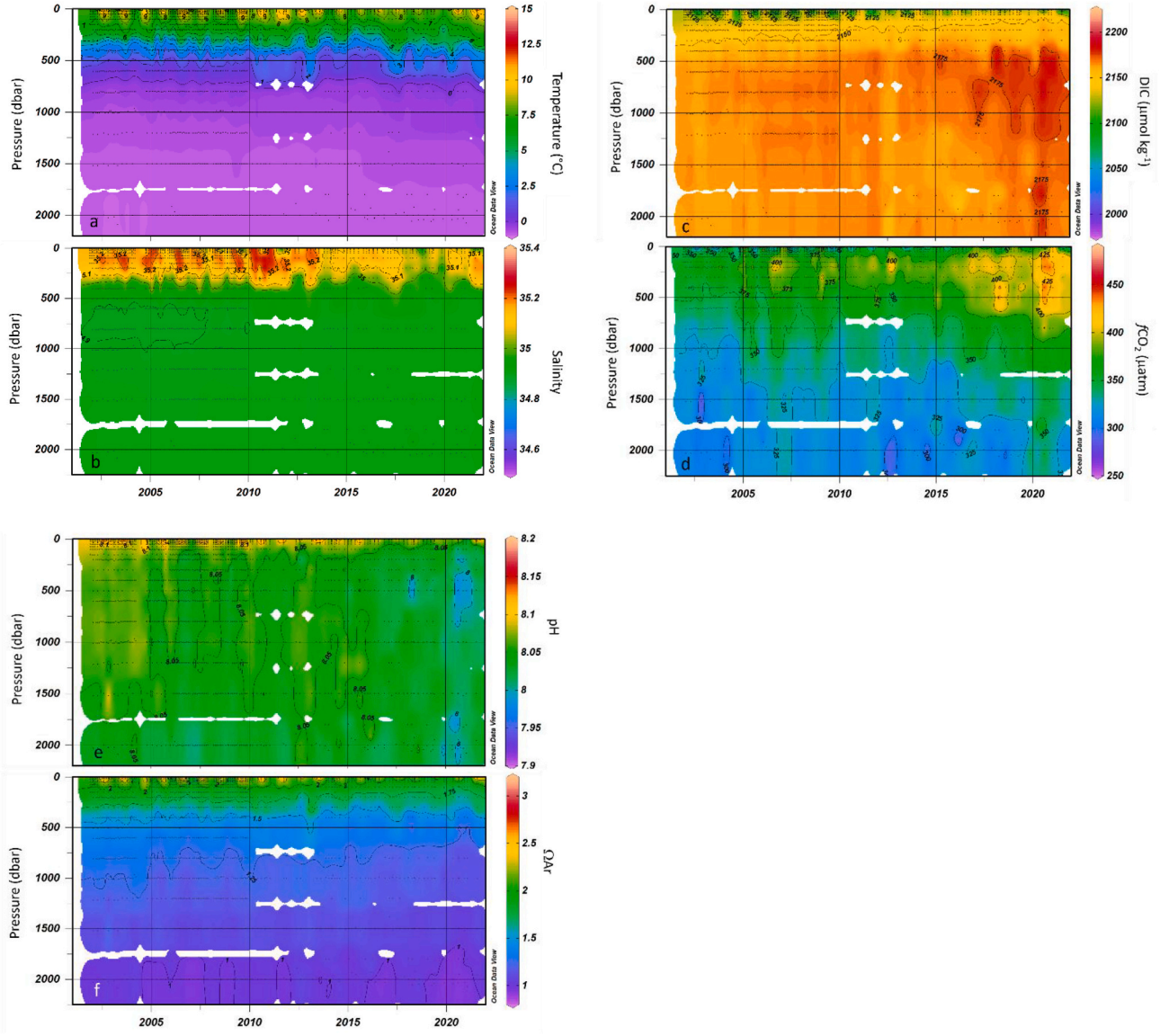

Fig. 4. Distribution of (a) temperature (°C), (b) salinity, (c) DIC (μmol kg^{-1}), (d) fCO_2 (μatm), (e) pH, and (f) Ω_{Ar} from the OWSM timeseries of discrete data between 2001 and 2021.

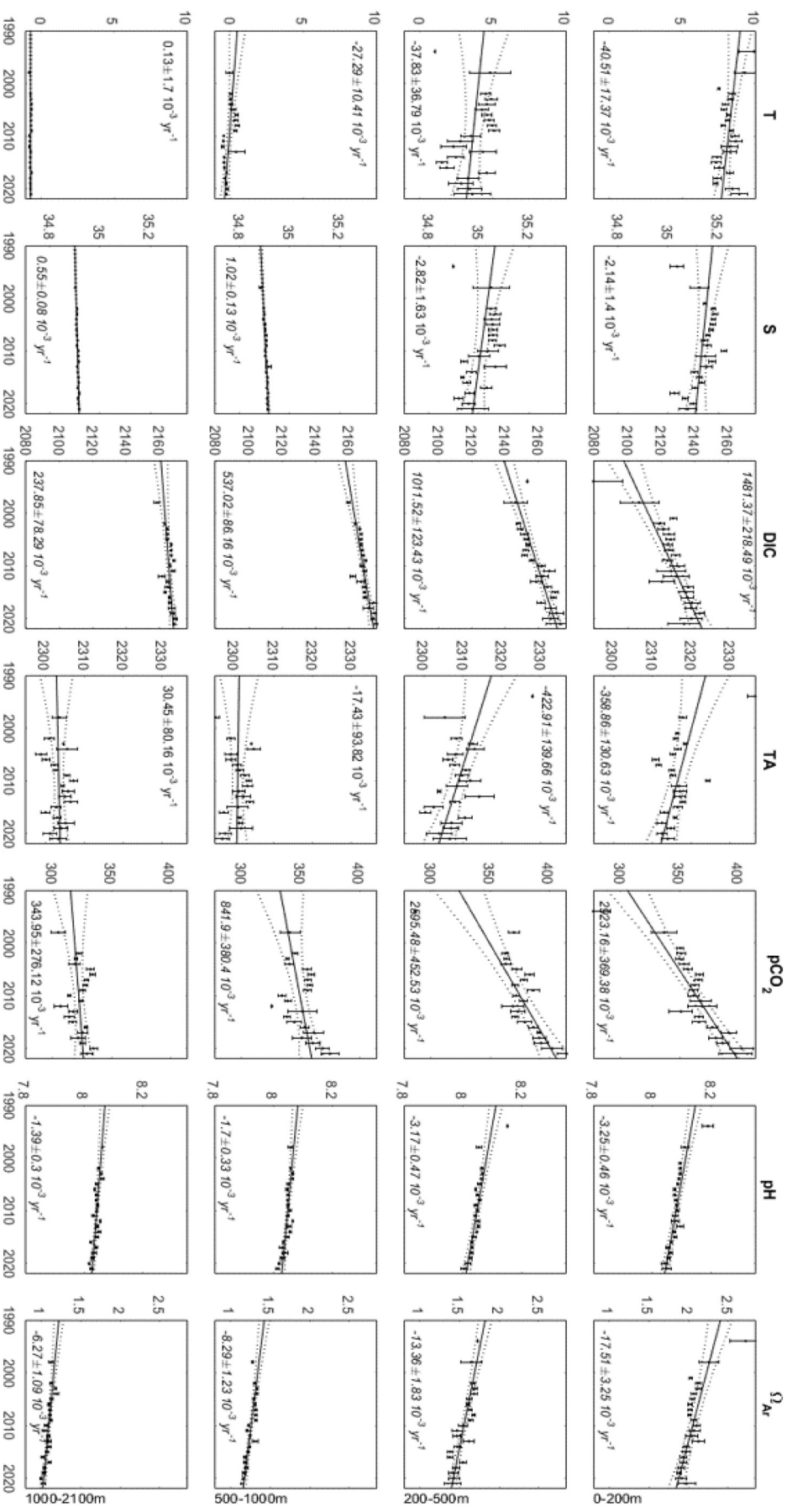

Fig. 5. Observed temperature (°C yr^{-1}), salinity (yr^{-1}), DIC (μmol kg^{-1} yr^{-1}), TA, (μmol kg^{-1} yr^{-1}), pCO_2 (μatm yr^{-1}), pH (yr^{-1}), and Ω_{Ar} (yr^{-1}) over 5 depth intervals at OWSM. Black dots with vertical error intervals are annual averages and standard deviation, solid black lines represent the overall trend during the period investigated, with the corresponding standard error. Dotted lines indicate the 95% confidence interval of the trend and numbers in cursive represent significant trends (see Table 2 for details).

Table 2
Trend values with corresponding standard error at different water depths at OWSM based on data between 1994 and 2021.

	0–200 m	200–500 m	500–1000 m	1000–2100 m
Temperature (°C yr^{-1})	***−0.041 ± 0.017***	−0.038 ± 0.037	***−0.027 ± 0.010***	0.0001 ± 0.002
Salinity (yr^{-1})	−0.002 ± 0.001	−0.003 ± 0.002	***0.001 ± 0.0001***	***0.0006 ± 0.00008***
DIC (µmol kg^{-1} yr^{-1})	***1.48 ± 0.22***	***1.01 ± 0.12***	***0.54 ± 0.09***	***0.24 ± 0.07***
TA (µmol kg^{-1} yr^{-1})	***−0.36 ± 0.13***	***−0.42 ± 0.14***	−0.02 ± 0.09	0.03 ± 0.08
fCO_2 (µatm yr^{-1})	***2.92 ± 0.37***	***2.60 ± 0.45***	***0.84 ± 0.38***	0.34 ± 0.28
pH (yr^{-1})	***−0.0033 ± 0.0005***	***−0.0032 ± 0.0005***	***−0.0017 ± 0.0003***	***−0.0014 ± 0.0003***
Ω_{Ar} (yr^{-1})	***−0.018 ± 0.003***	***−0.013 ± 0.002***	***−0.008 ± 0.001***	***−0.006 ± 0.001***

Bold and cursive numbers represent significant trends ($p < 0.05$).

measurements between 2007 and 2021 (2.69 ± 0.14 µatm; Fig. 3b). As expected, the trends (Fig. 5) weaken from the surface layer towards the deepest water layer, and at 1000–2100 m the DIC, fCO_2, pH, and Ω_{Ar} change by +0.24 ± 0.07 µmol kg^{-1} yr^{-1}, +0.34 ± 0.28 µatm yr^{-1}, −0.0014 ± 0.0003 yr^{-1}, and − 0.006 ± 0.001 yr^{-1}, respectively. The negative pH trend of the deepest layer at OWSM is less than half compared to that of the surface layer (−0.0033 yr^{-1}), while the corresponding relationship between deep and surface water Ω_{Ar} is approximately 1/3. Furthermore, at 1000–2100 m the annual averaged Ω_{Ar} is approaching undersaturated values. Over a narrower depth interval (1850–2100 m, not shown), the water is occasionally undersaturated with respect to aragonite, however, the fluctuations are large.

In general, the long-term trends calculated for various depth intervals in the current study (Fig. 5 and Table 2) are similar and within the uncertainty limits to those calculated for the Norwegian Sea by Fransner et al. (2021). They used data from a larger area in the Norwegian Sea (64–67.7°N, −3.4–3.3°E) and a longer time period (1981–2019) compared to our study, which allowed for more stations and more data in their study. In their study, data from and a TTO-NAS station (Transient Tracers in the Ocean - North Atlantic Study, e.g., Tanhua and Wallace, 2005) from 1981 and OWSM (2001–2019) were included. Discrepancies between the trends in the current study and that of Fransner et al. (2021) are, e.g., the pH trends at 200–500 m and 1000–2000 m depth, and the Ω_{Ar} trends deeper than 200 m, which all are significantly stronger in the current study. This difference is likely connected to more similar water masses having the same water history at the fixed OWSM compared to the larger Norwegian Basin area examined in Fransner et al. (2021) where water masses with different water histories are mixed. Furthermore, the pH trends at OWSM are similar to those from the Iceland Sea presented in Fransner et al. (2021), and similarities are also seen in DIC and fCO_2. The trend in Ω_{Ar}, on the contrary, is stronger at OWSM compared to that for the Iceland Sea, which is likely an effect of Ω_{Ar} being positively correlated to temperature while the opposite is the case for pH. The Iceland Sea warmed significantly over the period 1981–2019 (Fransner et al., 2021), which has counteracted decreasing Ω_{Ar} due to increased CO_2.

In the current work, we have included a few extra stations from OWSM from the 1990s, as these data are within 12 km from the fixed position of 66°N 2°E. Without these early data, the trend in pH over the years 2001–2021, is −0.0022 (not shown) based on annual averages within the 200 m upper layer, and this is comparable to the surface pH trends in the Lofoten Basin, Greenland Sea, and the Fram Strait (Fransner et al., 2021) and to that in the Irminger Sea (Bates et al., 2014). The annual pH over the years 1994–2021 has been examined by pieces, which reveals a varying strength of the trend over time, e.g., over the years 2002–2006 and 2013–2017 (Fig. S3) the pH trends were particularly strong, amounting to −0.0053 yr^{-1} (R^2 = 0.95) and −0.0098 yr^{-1} (R^2 = 0.93), respectively, while during the years 2006–2010 (Fig. S3) the pH trend was positive (+0.0023 yr^{-1}, $R^2 = 0.9$). Even if these time periods are short, the changing trends are still indicative of the highly variable nature of this ocean area and underpins the importance of long time series to be able to determine significant changes in the hydrographic system as well as the carbonate system.

Overall, the trends decrease as the depth increase (Fig. 5 and Table 2) since the strongest drivers for the observed change are found primarily in the shallowest water (see the section below on Drivers). However, the significant trends in DIC, fCO_2, pH, and Ω_{Ar} seen in intermediate water (Fig. 5 and Tables 2, 500–1000 m depth) is connected to advection from the Iceland and Greenland Sea, while the significant trends in DIC, pH, and Ω_{Ar} at 1000–2000 m depth (Fig. 5 and Table 2) is partly caused by influence from Greenland Sea deep water, and, to a larger extent, influence from the Arctic deep water (Østerhus and Gammelsrød, 1999; Blindheim and Østerhus, 2005).

The saturation horizon ($\Omega_{Ar} = 1$) fluctuates around 2000 m (median depth) over the years 2002–2021 (Fig. 4), with a significant negative trend in Ω_{Ar} over the depth layer 1000–2100 m. It is difficult to estimate the rate of shallowing of the saturation horizon, however, a coarse estimate of 7 m yr^{-1} is calculated based on an average Ω_{Ar} of 1 found at 1950 m depth in 2002 and at 1820 m depth in 2021. This is higher than the saturation horizon shoaling of 4 m yr^{-1} estimated for the Iceland Sea by Ólafsson et al. (2009), however, taking into consideration the high uncertainty of the OWSM estimate, the numbers are likely comparable.

Interestingly, the water column seems to have cooled significantly (−0.041 ± 0.017 °C yr^{-1} at surface and − 0.027 ± 0.010 °C yr^{-1} at 500–1000 m depth) since 1994, which is surprising. The semi-continuous surface temperature measurements from M/S Polarfront between 2006 and 2009 and from the Polarbuoy between 2011 and 2021 also showed a cooling, though not significant (0.0086 °C yr^{-1}). However, the temporal variability is large, and as an example, over the years 2004–2011, the temperature of the upper 200 m increased significantly (Fig. S3) with +0.13 ± 0.04 °C yr^{-1} (R^2 = 0.7), while during the years 2014–2017, the temperature increase was +0.29 ± 0.13 °C yr^{-1} ($R^2 = 0.7$). Even if warming of the North Atlantic Water is indisputable (e.g., Holliday et al., 2008; Mork et al., 2019), the high temporal variability is also commented in previous studies. Holliday et al. (2008) concluded that the temperature of the Atlantic inflow to the Nordic Seas has increased since the 1990s, but they also highlighted cooling of the water between the Faeroe-Shetland Channel and OWSM during 2002–2006. Furthermore, Mork et al. (2019) examined Norwegian Sea Argo data between 2002 and 2018 and they found that the water temperature increased between 2011 and 2018, while during the previous years the temperature anomalies varied between cold and warm periods. The temporal variability in temperature is briefly compared with the change in the NAO index (Hurrel, 2005), which is the difference between the normalized the sea-level pressure at Lisbon (PT) and Reykjavik (IS), where a positive NAO index is associated with warmer and wetter Northern Europe compared to negative NAO index, which reflect colder and drier northern Europe. Mork and Blindheim (2000) found a correlation between high winter (JFM) NAO index and a reduced westward extension of the Atlantic Water in the Norwegian Sea and, thus, increased influence of cold Arctic water. There is no clear correlation between the winter temperature (JFM) of the upper 200 m at OWSM and the winter NAO index, however, there seems to be a tendency of high winter NAO indexes occurring simultaneously with low temperature (Fig. S3) between 2007 and 2021.

Furthermore, there is no significant temperature change in the deepest layer (1000–2100 m) at OWSM, which is in contradiction to earlier studies in the area (e.g., Østerhus and Gammelsrød, 1999; Blindheim and Østerhus, 2005). Østerhus and Gammelsrød (1999) proved a warming of the deepest layer (~2000 m) at OWSM of 0.01 °C yr^{-1} between 1985 and 1997. The discrepancy between our study and that of Østerhus and Gammelsrød (1999) has several possible explanations. One explanation is that our trend analysis is based on a depth layer

of 1100 m, while Østerhus and Gammelsrød (1999) based their analysis on data primarily collected at 2000 m depth. Furthermore, their timeseries was based on a higher frequency of data (5 times a week) compared to our monthly data from 2002 to 2009 and 4–6 times per year after 2009. Lastly, there is only minor overlap between the timeseries used in the current work and that of Østerhus and Gammelsrød (1999), and, thus, there might be a possibility that the warming of the deep water has weakened. We checked the temperature trend in our timeseries data within a 250 m depth range from the bottom (data from 1850 to 2100 m depth; not shown), and this resulted in a significant warming of the depth layer of 0.0045 ± 0.0003 °C yr^{-1} over the years 1994–2021. This is in line with the warming described in Østerhus and Gammelsrød (1999), but still weaker than they observed.

OWSM have evidenced that the sea surface CO_2 in the area increases faster than that of the atmosphere.

To further investigate the driving processes for the observed change in pH, we first examined the freshwater effect. The TA and DIC were salinity normalized by using the approach from Friis et al. (2003) where the salinity normalized TA (nTA) is defined as:

$$nTA = \frac{TA_{meas} - TA_{S=0}}{S_{meas}} 35 + TA_{S=0} \quad (4)$$

The term $TA_{S=0}$ is determined from Nondal et al. (2009) and equals 582 (for salinities >34.5, which is the case for basically all OWSM data). nDIC is determined as above by replacing TA with DIC. Furthermore, Eq. 5 is used where the DIC and TA terms are split into contribution from freshwater (*fw*) and biogeochemistry (*bg*):

$$\frac{\partial[H^+]}{\partial DIC}\frac{dDIC}{dt} + \frac{\partial[H^+]}{\partial TA}\frac{dTA}{dt} = \frac{\partial[H^+]}{\partial DIC_{fw}}\frac{dDIC_{fw}}{dt} + \frac{\partial[H^+]}{\partial TA_{fw}}\frac{dTA_{fw}}{dt} + \frac{\partial[H^+]}{\partial DIC_{bg}}\frac{dDIC_{bg}}{dt} + \frac{\partial[H^+]}{\partial TA_{bg}}\frac{dTA_{bg}}{dt} \quad (5)$$

5.4. Drivers of the observed trends

The drivers of the observed long-term trends in pH have been explored by using the decomposition approach with respect to $[H^+]$ as described in Eq. 3 where changes in temperature (T), salinity (S), DIC and TA are assumed to influence the observed changes in $[H^+]$ and, thus, also pH. The annual observed change in $[H^+]$ and drivers of the $[H^+]$ change are shown in Fig. S4, while the corresponding results in pH are presented in Fig. 6a, where the bars represent annual changes in pH due to changes in each of the drivers (see Table 3). The analysis shows that for all depth layers, increasing DIC is the major driver for the decrease in pH (shown as the largest bars of the drivers in the plot). Change in temperature and TA counteract each other and result in no net change in pH. Furthermore, the sum of driver induced pH changes (SUM) equals the pH change calculated based on observations (OBS), at least for the upper 1000 m. This indicates that it is realistic to assume temperature, salinity, DIC and TA to be the drivers for pH changes in these waters. Deeper than 1000 m the assumption of Eq. 3 and 4 does not seem to hold, which could be connected to a combination of uncertainties in the decomposition approach and processes excluded by this approach. Deeper than 1000 m, primarily Norwegian Sea Deep water is found. As mentioned above, the deep water in the Norwegian Sea seems to be replaced with increasing amount of deep and relatively warm water from the Arctic and less so from the relatively cold Greenland Sea (Østerhus and Gammelsrød, 1999). Our decomposition method does not specifically calculate the contribution from advection; however, the process is to some extent included as it affects the rate of change in the drivers. It is likely that advection is the dominating process in the deepest layer of the Norwegian Sea basin.

DIC changes, being the primary driver for the pH trend, are influenced by air-sea gas exchange, biological activity, vertical mixing, and advection, and all these processes except air-sea gas exchange also affect TA. If air-sea gas exchange was the only process and the CO_2 increase in surface ocean was similar to that of the atmosphere, the pH trend would have been approximately half of the observed value (Fig. 6a, crosses in the upper panel). However, the semi-continuous measurements at

where both $dDIC_{fw}/dt$ and dTA_{fw}/dt are assumed approximately equal to dS/dt. The biogeochemistry term (*bg*) in Eq. 5 is determined from nTA and nDIC and still comprises contribution from air-sea gas exchange, biological activity, vertical mixing, and advection. In more detail, the terms are determined the following way:

$$\frac{\partial[H^+]}{\partial DIC_{fw}}\frac{dDIC_{fw}}{dt} = \frac{\partial[H^+]}{\partial(DIC - nDIC)}\frac{dS}{dt} \quad (6)$$

$$\frac{\partial[H^+]}{\partial TA_{fw}}\frac{dTA_{fw}}{dt} = \frac{\partial[H^+]}{\partial(TA - nTA)}\frac{dS}{dt} \quad (7)$$

$$\frac{\partial[H^+]}{\partial DIC_{bg}}\frac{dDIC_{bg}}{dt} = \frac{\partial[H^+]}{\partial nDIC}\frac{dnDIC}{dt} \quad (8)$$

$$\frac{\partial[H^+]}{\partial nTA}\frac{dnTA}{dt} = \frac{\partial[H^+]}{\partial nTA}\frac{dnTA}{dt} \quad (9)$$

As previously, $[H^+]$ changes are converted to pH changes. Fig. 6b and Table 3 show that the freshwater component of DIC and TA are small for all depth layers. Furthermore, the sum of the drivers (SUM) is similar to the pH change from observations (OBS) at the depth 200–500 m, but less so for the remaining depths.

Furthermore, we examine how changes in biological activity, i.e., primary production/remineralization and production/dissolution of calcium carbonate shells and skeletons will affect the pH. We assume that DIC_{bg} and TA_{bg} represents all the biological activity which are split into carbon fixation in organic material during primary production (called "soft" in the equations below) and carbon fixation into shells and skeleton (called "hard" in the equations below), and thus, the DIC_{bg} and TA_{bg} terms in Eq. 5 are written as:

$$\frac{\partial[H^+]}{\partial DIC_{bg}}\frac{dDIC_{bg}}{dt} + \frac{\partial[H^+]}{\partial TA_{bg}}\frac{dTA_{bg}}{dt} = \frac{\partial[H^+]}{\partial DIC_{soft}}\frac{dDIC_{soft}}{dt} + \frac{\partial[H^+]}{\partial DIC_{hard}}\frac{dDIC_{hard}}{dt} + \frac{\partial[H^+]}{\partial TA_{soft}}\frac{dTA_{soft}}{dt} + \frac{\partial[H^+]}{\partial TA_{hard}}\frac{dTA_{hard}}{dt} \quad (10)$$

Carbon fixed into organic material (DIC_{soft} and TA_{soft}) is determined by assuming that:

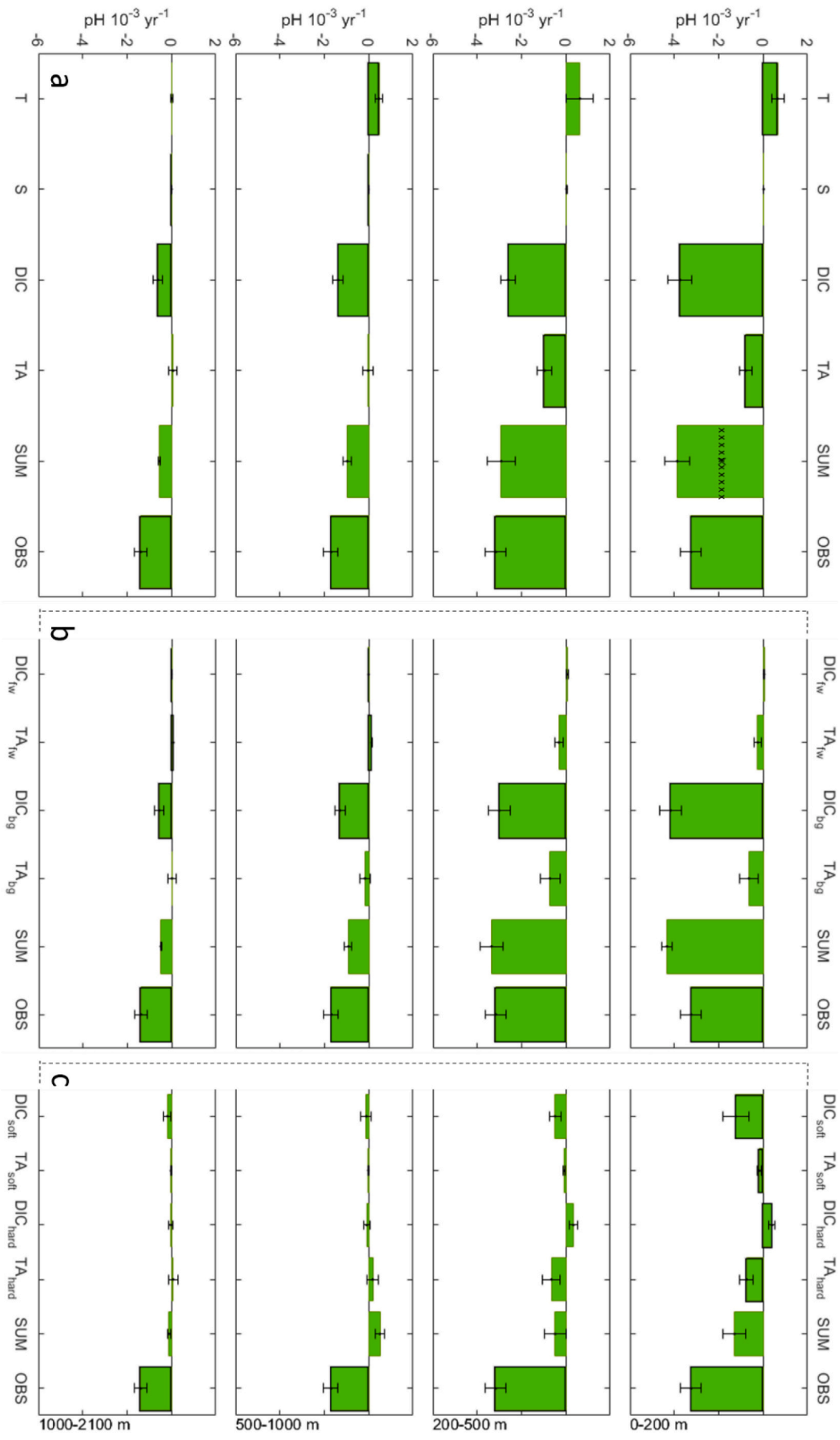

(caption on next page)

Fig. 6. Estimated drivers of annual change in pH (1994–2021) at various depth intervals. Histograms show pH change for each driving factor, with standard error. Significant (at 95% confidence level) changes in pH are encircled with a black line. SUM is the accumulated effect of all drivers, while OBS (observed) refers to the calculated pH trend from observed data. a) The drivers are split into temperature (T), salinity (S), Dissolved Inorganic Carbon (DIC), and total alkalinity (TA). Crosses show expected level of change in pH where increase in atmospheric CO_2 is the only driver; b) the drivers are split into T, S (see panel a for these two drivers), freshwater component of DIC (DIC_{fw}) and TA (TA_{fw}), and primary production component of DIC (DIC_{bg}) and TA (TA_{bg}); c) the drivers are split into T, S, freshwater component of DIC (DIC_{fw}) and TA (TA_{fw}) (see panel a and b for these fours drivers), soft tissue component of DIC (DIC_{soft}), soft tissue component of TA (TA_{soft}), calcium carbonate component of DIC (DIC_{hard}), and calcium carbonate component of TA (TA_{hard}). See Results and discussion for detailed explanation.

Table 3
Contribution to the pH trend from various variables.

Effect on pH trend from change in	0–200 m	200–500 m	500–1000 m	1000–21,000 m
DIC (10^{-3} yr^{-1})	***−3.9 ± 0.6***	***−2.7 ± 0.3***	***−1. 4 ± 0.2***	***−0.6 ± 0.2***
DIC_{fw} (10^{-3} yr^{-1})	0.04 ± 0.03	0.05 ± 0.03	***−0.019 ± 0.003***	***−0.010 ± 0.001***
DIC_{bg} (10^{-3} yr^{-1})	***−4.2 ± 0.5***	***−3.0 ± 0.5***	***−1. 3 ± 0.2***	***−0.6 ± 0.2***
DIC_{soft} (10^{-3} yr^{-1})	***−1. 2 ± 0.6***	−0.5 ± 0.3	−0.1 ± 0.2	−0.2 ± 0.2
DIC_{hard} (10^{-3} yr^{-1})	***0.4 ± 0.2***	0.3 ± 0.2	−0.1 ± 0.1	−0.04 ± 0.11
TA (10^{-3} yr^{-1})	***−0.9 ± 0.3***	***−1.1 ± 0.4***	−0.04 ± 0.24	0.08 ± 0.21
TA_{fw} (10^{-3} yr^{-1})	−0.3 ± 0.2	−0.3 ± 0.2	***0.12 ± 0.02***	***0.064 ± 0.009***
TA_{bg} (10^{-3} yr^{-1})	−0.6 ± 0.4	−0.7 ± 0.4	−0.2 ± 0.2	0.009 ± 0.2
TA_{soft} (10^{-3} yr^{-1})	***−0.18 ± 0.09***	−0.07 ± 0.04	−0.02 ± 0.03	−0.03 ± 0.02
TA_{hard} (10^{-3} yr^{-1})	***−0.8 ± 0.3***	−0.7 ± 0.4	0.2 ± 0.3	0.07 ± 0.21

The numbers represent annual pH change ± standard error. Bold and cursive numbers represent significant trends ($p < 0.05$).

$$DIC_{soft} = a\left(NO_3 - NO_{3\ pref}\right) \tag{11}$$

$$TA_{soft} = -1.36\left(NO_3 - NO_{3\ perf}\right) \tag{12}$$

where a is the stoichiometric ratio $C{:}N = 6.6 \pm 0.1$ ($R^2 = 0.71$), which is determined from OWSM data deeper than 25 m. The coefficient 1.36 is included to account for TA contribution from the oxidation of organic nitrogen, phosphorous, and sulphur according to Wolf-Gladrow et al. (2007). The term $NO_{3\ perf}$ is the *preformed* nitrate concentration, here taken from the preformed nutrients fields by Carter et al. (2021). We use the 1°x1° covering the OWSM location. The preformed nitrate value is defined as the nitrate concentration in seawater when it was last at surface, which in the ocean interior change only as a result of advection and mixing. Thus, changes in DIC_{soft} and TA_{soft} represent only changes due to biotic processes. Further, changes in DIC and TA due to formation and dissolution of calcium carbonate shells and skeletons are determined by 1) using the fact that when calcium carbonate is formed, TA and DIC are reduced in the rate 2:1, i.e., DIC_{hard} equals half that of TA_{hard} (e.g., Zeebe and Wolf-Gladrow, 2001) and 2) TA_{hard} is determined as the residual after subtracting TA_{soft} and preformed TA (TA_{pref}) from the observed TA:

$$DIC_{hard} = 0.5(TA_{hard}) \tag{13}$$

$$TA_{hard} = TA - TA_{soft} - TA_{pref} \tag{14}$$

Here TA_{pref} is the preformed total alkalinity, which is also extracted from the Carter et al. (2021) product. [H^+] changes are converted to pH changes, and the results of the decomposition analysis are shown if Fig. 6c and Table 3. The most prominent result is that the sum of the driver induced pH changes (SUM) differs substantially from the observed pH change (OBS), and thus, our assumption presented in Eq. 10 does not tell the whole story. The reason for this is that the latter decomposition approach neither includes air-sea gas exchange, vertical mixing nor advection. Despite the uncertainties, the TA induced change in pH (Fig. 6a) is relatively similar to the sum of pH change driven by changes in TA_{fw}, TA_{soft}, TA_{hard} (Fig. 6b and c), and thus, it is reasonable to assume that neither vertical mixing nor advection influence the pH trend to a noticeable degree. Therefore, the effect of air-sea gas exchange can be estimated by subtracting the pH changes driven by DIC_{fw}, DIC_{soft} and DIC_{hard} from the pH changes driven by DIC. Thus, the surface pH trend driven by uptake of atmospheric CO_2 amounts to −0.0031 yr^{-1}, which represents as much as 80% of the total DIC induced change in pH. As expected, the major part of the pH trend is driven by uptake of atmospheric CO_2, however, previously, the actual amount has not been quantified. The remaining change in DIC over the years is primarily due to changes in primary production and remineralization. However, the variability of biological production is high from year to year and is in general dependent on physical factors like transport of water into the Nordic seas, solar radiation, sea ice, and the North Atlantic Oscillation (Skogen et al., 2007). Thus, future climate will be an important factor for how much biological material will be produced and obviously, future climate will be vital for how the trend in pH will develop.

6. Conclusion

Time series data from Ocean Weather Station M (OWSM) in the Norwegian Sea collected with a variety of frequencies and from a variety of platforms are used to examine the inorganic carbon cycle over the years 1994–2021. From semi-continuous CO_2 measurements, the winter surface fCO_2 is increasing at a higher speed (2.69 μatm yr^{-1}) than that of the atmosphere (2.27 μatm yr^{-1}), and thus, the area appears to be a decreasing sink for atmospheric CO_2. This might be explained by a reduced buffer capacity, which results in a higher content of CO_2 in the Atlantic Water entering the Nordic Seas from the south. If this continues, the sea surface in this area could turn into a source for atmospheric CO_2 in the future. Furthermore, over the years 1994–2021 the pH and Ω_{Ar} of the surface water have decreased significantly with −0.0033 ± 0.0005 yr^{-1} and −0.018 ± 0.003 yr^{-1}, respectively. This pH change amounts to 0.092 over the 28 years of study, which is comparable to the global pH decrease (0.1) since the onset of industrial revolution. Thus, ocean acidification it is occurring at a faster rate in the Norwegian Sea compared to the global average.

Significant ocean acidification is also seen in the deepest layer at OWSM (1000–2100 m) with pH and Ω_A values of −0.0014 ± 0.0003 yr^{-1} and −0.006 ± 0.001 yr^{-1}, respectively. The saturation horizon at the station fluctuates irregularly over the period 1994–2021 and a rough estimate indicate that the horizon has shoaled by 7 m yr^{-1} over this period of nearly three decades.

Based on decomposition analysis, changes in DIC are determined to be the primary cause for the negative trend in pH. These DIC changes are primarily due to uptake of atmospheric CO_2, but also changes in the primary production/remineralization plays a role. This work proves the importance of long and sustained time series for identifying and quantifying changes in the biogeochemistry and climate.

Declaration of Competing Interest

The authors declare that they have no known competing financial interests or personal relationships that could have appeared to influence the work reported in this paper.

Data availability

The surface data is available in SOCAT (www.socat.info). The water column data will be available in GLODAPv2.2022.

Acknowledgements

This work has received contributions from the Research Council Norway, the Norwegian Environment Agency, the Geophysical Institute at the University of Bergen (GFI-UoB), and the Institute of Marine Research (IMR). The authors are grateful to the captains and crews at the M/S Polarfront and to the kind help from crew members at the research vessel fleet of the Norwegian Institute of Marine Research. Furthermore, we would like to thank the engineers at GFI-UiB, who have analysed the discrete carbon samples and who have, together with engineers from IMR, contributed to setup, deployment, retrieval, and maintenance of the surface buoy.

Appendix A. Supplementary data

Supplementary data to this article can be found online at https://doi.org/10.1016/j.jmarsys.2022.103775.

References

Azetsu-Scott, K., Clarke, A., Falkner, K., Hamilton, J., Jones, E.P., Lee, C., Petrie, B., Prinsenberg, S., Starr, M., Yeats, P., 2010. Calcium carbonate saturation states in the waters of the Canadian Arctic Archipelago and the Labrador Sea. J. Geophys. Res. 115, C11021. https://doi.org/10.1029/2009JC005917.

Bakker, D.C.E., et al., 2016. A multi-decade record of high-quality fCO_2 data in version 3 of the Surface Ocean CO_2 Atlas (SOCAT). Earth Syst. Sci. Data 8, 383–413. https://doi.org/10.5194/essd-8-383-2016.

Bates, N.R., Astor, Y.M., Church, M.J., Currie, K., Dore, J.E., González-Dávila, M., Lorenzoni, L., Muller-Karger, F., Olafsson, J., Santana-Casiano, J.M., 2014. A time-series view of changing ocean chemistry due to ocean uptake of anthropogenic CO2 and ocean acidification. Oceanography 27 (1), 126–141. https://doi.org/10.5670/oceanog.2014.16.

Blindheim, J., Østerhus, S., 2005. The Nordic seas, main oceanographic features. In: Drange, H., Dokken, T., Furevik, T., Gerdes, R., Berger, W. (Eds.), The Nordic Seas: An Integrated Perspective, Vol. 158 of Geophysical Monograph Series. American Geophysical Union, Washington DC, pp. 11–38.

Carter, B.R., Feely, R.A., Lauvset, S.K., Olsen, A., DeVries, T., Sonnerup, R., 2021. Preformed properties for marine organic matter and carbonate mineral cycling quantification. Glob. Biogeochem. Cycles 35. https://doi.org/10.1029/2020GB006623.

Chierici, M., Fransson, A., 2009. CaCO3 saturation in the surface water of the Arctic Ocean: undersaturation in freshwater influenced shelves. Biogeosciences 6, 2421–2432. https://doi.org/10.5194/bg-6-2421-2009.

Currie, K.I., Reid, M.R., Hunter, K.A., 2011. Interannual variability of carbon dioxide drawdown by subantarctic surface water near New Zealand. Biogeochemistry 104, 23–34. https://doi.org/10.1007/s10533-009-9355-3.

Dale, T., Rey, F., Heimdal, B.R., 1999. Seasonal development of phytoplankton at a high latitude oceanic site. Sarsia 84, 419–435.

Dickson, A.G., 1990. Standard potential of the reaction: AgCl(s) + 1/2H2(g) = Ag(s) + HCl(aq), and the standard acidity constant of the ion HSO4 – in synthetic sea water from 273.15 to 318.15 K. J. Chem. Thermodyn. 22, 113–127.

Dickson, A.G., Sabine, C.L., Christian, J.C., 2007. Guide to Best Practices for Ocean CO2 Measurements. British Columbia, North Pacific Marine Science Organization, PICES Special Publication, Sidney, p. 3.

Dlugokencky, E.J., Mund, J.W., Crotwell, A.M., Crotwell, M.J., Thoning, K.W., 2021. Atmospheric Carbon Dioxide Dry Air Mole Fractions from the NOAA GML Carbon Cycle Cooperative Global Air Sampling Network, 1968-2019, Version: 2021-02. https://doi.org/10.15138/wkgj-f215.

Doney, S.C., Fabry, V.J., Feely, R.A., Kleypas, J.A., 2009. Ocean acidification: the other CO2 problem. Annu. Rev. Mar. Sci. 1, 169–192. https://doi.org/10.1146/annurev.marine.010908.163834, pMID: 21141034.

Findlay, H.S., Tyrrell, T., Bellerby, R.G.J., Merico, A., Skjelvan, I., 2008. Carbon and nutrient mixed layer dynamics in the Norwegian Sea. Biogeosci. 5, 1395–1410.

Fransner, F., Fröb, F., Tjiputra, J., Chierici, M., Fransson, A., Goris, N., Jeansson, E., Johannessen, T., Jones, E., Lauvset, S.K., Ólafsdóttir, S.R., Omar, A., Skjelvan, I., Olsen, A., 2021. Nordic seas acidification. Biogeosci. Discuss. https://doi.org/10.5194/bg-2020-339, in review.

Friederich, G.E., Brewer, P.G., Herlien, R., Chavez, F.P., 1995. Measurement of sea surface partial pressure of CO2 from a moored buoy. Deep-Sea Res. I 42, 1175–1186. https://doi.org/10.1016/09670637(95)00044-7.

Friedlingstein, P., et al., 2020. Global carbon budget 2020. Earth Syst. Sci. Data 12, 3269–3340. https://doi.org/10.5194/essd-12-3269-2020.

Frigstad, H., Henson, S.A., Hartman, S.E., Omar, A.M., Jeansson, E., Cole, H., Pebody, C., Lampitt, R.S., 2015. Links between surface productivity and deep ocean particle flux at the Porcupine Abyssal Plain sustained observatory. Biogeosciences 12, 5885–5897. https://doi.org/10.5194/bg-12-5885-2015.

Friis, K., Körtzinger, A., Wallace, D.W.R., 2003. The salinity normalization of marine inorganic carbon chemistry data. Geophys. Res. Lett. 30 (2), 1085. https://doi.org/10.1029/2002GL015898.

Gattuso, J.-P., Hansson, L., 2012. Ocean acidification: background and history. In: Gattuso, J.-P., Hansson, L. (Eds.), Ocean Acidification. Oxford University Press.

Gattuso, J.-P., Lavigne, H., 2009. Technical note: approaches and software tools to investigate the impact of ocean acidification. Biogeosciences 6, 2121–2133.

González-Pola, C., Larsen, K.M.H., Fratantoni, P., Beszczynska-Möller, A. (Eds.), 2020. ICES Report on Ocean Climate 2019. https://doi.org/10.17895/ices.pub.7537. ICES Cooperative Research Reports No. 350. 136 pp.

Gundersen, et al., 2021. Declining silicate and nitrate concentrations in the northern North Atlantic. In: Karina von Schuckmann et al. (2021) Copernicus Marine Service Ocean State Report, Issue 5. J. Operat. Oceanogr. 14 (Sup 1), 1–185. https://doi.org/10.1080/1755876X.2021.1946240.

Hansen, B., Østerhus, S., 2000. North Atlantic–Nordic Seas exchanges. Prog. Oceanogr. 45, 109–208. https://doi.org/10.1016/S0079-6611(99)00052-X.

Haraldsson, C., Anderson, L.G., Hassellöv, M., Hulth, S., Olsson, K., 1997. Rapid, high-precision potentiometric titration of alkalinity in ocean and sediment pore waters. Deep-Sea Res. I 44, 2031–2044.

Hartman, S.E., Jiang, Z.-P., Turk, D., Lampitt, R.S., Frigstad, H., Ostle, C., Schuster, U., 2015. Biogeochemical variations at the porcupine abyssal plain sustained observatory in the Northeast Atlantic Ocean, from weekly to inter-annual timescales. Biogeosciences 12, 845–853. https://doi.org/10.5194/bg-12-845-2015.

Holliday, N.P., Hughes, S.L., Bacon, S., Beszczynska-Möller, A., Hansen, B., Lavín, A., Loeng, H., Mork, K.A., Østerhus, S., Sherwin, T., Walczowski, W., 2008. Reversal of the 1960s to 1990s freshening trend in the Northeast North Atlantic and Nordic seas. Geophys. Res. Lett. 35 https://doi.org/10.1029/2007GL032675.

Hurrel, J.W., 2005. Decadal trends in the North Atlantic oscillation: regional temperatures and precipitation. Science 269, 676–679.

Jeansson, E., Olsen, A., Jutterström, S., 2017. Arctic intermediate water in the Nordic seas, 1991-2009. Deep-Sea Res. I 28, 82–97. https://doi.org/10.1016/j.dsr.2017.08.013.

Johnson, K.M., Wills, K.D., Butler, D.B., Johnson, W.K., Wong, C.S., 1993. Coulometric total carbon dioxide analysis for marine studies. Mar. Chem. 44, 167–187.

Kleypas, J.A., Feely, R.A., Fabry, V.J., Langdon, C., Sabine, C.L., Robbins, L.L., 2006. Impacts of Ocean Acidification on Coral Reefs and Other Marine Calcifiers: A Guide for Future Research, Report of a Workshop Held 18–20 April 2005, St. Petersburg, FL, Sponsored by NSF, NOAA, and the U.S. Geological Survey, 88 pp.

Lueker, T.J., Dickson, A.G., Keeling, C.D., 2000. Ocean pCO_2 calculated from dissolved inorganic carbon, alkalinity, and equations for K_1 and K_2: validation based on laboratory measurements of CO_2 in gas and seawater at equilibrium. Mar. Chem. 70, 105–119.

Metzl, N., Corbière, A., Reverdin, G., Lenton, A., Takahashi, T., Olsen, A., Johannessen, T., Pierrot, D., Wanninkhof, R., Ólafsdóttir, S.R., Olafsson, J., Ramonet, M., 2010. Recent acceleration of the sea surface fCO2 growth rate in the North Atlantic subpolar gyre (1993–2008) revealed by winter observations. Glob. Biogeochem. Cycles 24. https://doi.org/10.1029/2009GB003658.

Mintrop, L., Pérez, F., González-Dávila, M., Santana-Casiano, J., Körtzinger, A., 2000. Alkalinity determination by potentiometry: Intercalibration using three different methods. Cienc. Mar. 26, 23–37.

Moore, C.M., Mills, M.M., Milne, A., Langlois, R., Achterberg, E.P., Lochte, K., Eider, R.J. G., La Roche, J., 2006. Iron limits primary productivity during spring bloom development in the Central North Atlantic. Glob. Change Bio. 12, 626–634.

Mork, K.A., Blindheim, J., 2000. Variations in the Atlantic inflow to the Nordic Seas, 1955-1996. Deep-Sea Res. I 47, 1035–1057.

Mork, K.A., Skagseth, Ø., Søiland, H., 2019. Recent warming and freshening of the Norwegian Sea observed by Argo data. J. Clim. 32 https://doi.org/10.1175/JCLI-D-18-0591.1.

Mosby, H., 1962. Water, salt, and heat balance of the North Polar Sea and of the Norwegian Sea. Geophys. Nor. 24 (11), 289–313.

Mucci, A., 1983. The solubility of calcite and aragonite in seawater at various salinities, temperatures and at one atmosphere pressure. Am. J. Sci. 283, 780–799. https://doi.org/10.2475/ajs.283.7.780.

Nilsen, E.Ø., Falck, E., 2006. Variations of mixed layer properties in the Norwegian Sea for the period 1948-1999. Prog. Oceanogr. 70, 58–90. https://doi.org/10.1016/j.pocean.2006.03.014.

Nondal, G., Bellerby, R.G.J., Olsen, A., Johannessen, T., Olafsson, J., 2009. Optimal evaluation of the surface ocean CO2 system in the northern North Atlantic using data from voluntary observing ships. Limnol. Oceanogr. Methods 7, 109–118.

Ólafsson, J., Ólafsdóttir, S.R., Benoit-Cattin, A., Danielsen, M., Arnarson, T.S., Takahashi, T., 2009. Rate of Iceland Sea acidification from time series measurements. Biogeosciences 6, 2661–2668. https://doi.org/10.5194/bg-6-2661-2009.

Olafsson, J., Olafsdottir, S.R., Benoit-Cattin, A., Takahashi, T., 2010. The Irminger Sea and the Iceland Sea time series measurements of sea water carbon and nutrient chemistry 1983–2006. Earth Syst. Sci. Data 2, 99–104. https://doi.org/10.5194/essd-2-99-2010.

Olsen, A., 2009. Nordic seas total alkalinity data in CARINA. Earth Syst. Sci. Data 1, 77–86.

Olsen, A., Omar, A.M., Bellerby, R.G.J., Johannessen, T., Ninnemann, U., Brown, K.R., Olsson, K.A., Ólafsson, J., Nondal, G., Kivimäe, C., Kringstad, S., Neill, C., Ólafsdóttir, S., 2006. Magnitude and origin of the anthropogenic CO2 increase and

13C Suess effect in the Nordic seas since 1981. Global Biogeochem. Cycl. 20 https://doi.org/10.1029/2005GB002669.

Olsen, A., et al., 2020. GLODAPv2.2020 - the second update of GLODAPv2. Earth Syst. Sci. Data 12, 3653–3678. https://doi.org/10.5194/essd-12-3653-2020.

Orr, J.C., Epitalon, J.-M., Dickson, A.G., Gattuso, J.-P., 2018. Routine uncertainty propagation for the marine carbon dioxide system. Marine Cemistry 207, 84–107. https://doi.org/10.1016/j.marchem.2018.10.006.

Orvik, K.A., Skagseth, Ø., Mork, M., 2001. Atlantic inflow to the Nordic seas: current structure and volume fluxes from moored current meters, VM-ADCP and SeaSoar-CTD observations, 1995-1999. Deep-Sea Res. I 48, 937–957.

Østerhus, S., Gammelsrød, T., 1999. The abyss of the Nordic seas is warming. J. Clim. 2, 3297–3304.

Pierrot, D., Neill, C., Sullivan, K., Castle, R., Wanninkhof, R., Lüger, H., Johannessen, T., Olsen, A., Feely, R.A., Cosca, C.E., 2009. Recommendations for autonomous underway pCO2 measuring systems and data-reduction routines. Deep-Sea Res. II 56, 512–522.

Skjelvan, I., Falck, E., Rey, F., Kringstad, S., 2008. Inorganic carbon time series at ocean Weather Station M in the Norwegian Sea. Biogeoscience 5, 549–560. https://doi.org/10.5194/bg-5-549-2008.

Skogen, M.D., Budgell, W.P., Rey, F., 2007. Interannual variability in Nordic seas primary production. ICES J. Mar. Sci. 64, 889–898.

Steinacher, M., Joos, F., Frölicher, T.L., Plattner, G.-K., Doney, S.C., 2009. Imminent Ocean acidification in the Arctic projected with the NCAR global coupled carbon cycle-climate model. Biogeosciences 6, 515–533. http://www.biogeosciences.net/6/515/2009/.

Sutton, A.J., Sabine, C.L., Maenner-Jones, S., Lawrence-Slavas, N., Meinig, C., Feely, R. A., Mathis, J.T., Musielewicz, S., Bott, R., McLain, P.D., Fought, J., Kozyr, A., 2014. A high-frequency atmospheric and seawater pCO_2 data set from 14 open ocean sites using a moored autonomous system. Earth Syst. Sci. Data 6, 353–366. https://doi.org/10.5194/essd-6-353-2014.

Tanhua, T., Wallace, D.W.R., 2005. Consistency of TTO-NAS inorganic carbon data with modern measurements. Geophys. Res. Lett. 32, L14618. https://doi.org/10.1029/2005GL023248.

Tans, P.P., Conway, T.J., 2005. Monthly atmospheric CO2 mixing ratios from the NOAA CMDL carbon cycle cooperative global air sampling network, 1968–2002. In: Trends: A Compendium of Data on Global Change. Carbon Dioxide Information Analysis Center, Oak Ridge National Laboratory, US Department of Energy, Oak Ridge, Tenn., U.S.A.

Uppström, L.R., 1974. The boron/chlorinity ratio of deep-sea water from the Pacific Ocean. Deep-Sea Res. Oceanogr. Abstr. 21 (2), 161–162.

van Heuven, S., Pierrot, D., Rae, J.W.B., Lewis, E., Wallace, D.W.R., 2011. MATLAB Program Developed for CO2 System Calculations. ORNL/CDIAC-105b. Carbon Dioxide Information Analysis Center, Oak Ridge National Laboratory, U.S. Department of Energy, Oak Ridge, Tennessee. https://doi.org/10.3334/CDIAC/otg.CO2SYS_MATLAB_v1.1.

Wolf-Gladrow, D.A., Zeebe, R.E., Klaas, C., Körtzinger, A., Dickson, A.G., 2007. Total alkalinity: the explicit conservative expression and its application to biogeochemical processes. Mar. Chem. 106 (1–2 SPEC. ISS), 287–300. https://doi.org/10.1016/j.marchem.2007.01.006.

Zeebe, R.E., Wolf-Gladrow, D., 2001. CO2 in Seawater: Equilibrium, Kinetics, Isotopes. In: Elsevier Oceanography Series, Vol. 65. ISBN 0444505792.